DOI: 10.1002/chem.200600719

Solvent Polarity Controls the Helical Conformation of Short Peptides Rich in C^{α}-Tetrasubstituted Amino Acids

Massimo Bellanda,[a] Stefano Mammi,*[a] Silvano Geremia,[b] Nicola Demitri,[b] Lucio Randaccio,*[b] Quirinus B. Broxterman,[c] Bernard Kaptein,[c] Paolo Pengo,[a] Lucia Pasquato,*[b] and Paolo Scrimin*[a]

Abstract: The two peptides, rich in C^{α}-tetrasubstituted amino acids, Ac-[Aib-L-(αMe)Val-Aib]$_2$-L-His-NH_2 (**1**) and Ac-[Aib-L-(αMe)Val-Aib]$_2$-O-*t*Bu (**2a**) are prevalently helical. They present the unique property of changing their conformation from the α- to the 3_{10}-helix as a function of the polarity of the solvent: α in more polar solvents, 3_{10} in less polar ones. Conclusive evidence of this reversible change of conformation is reported on the basis of the circular dichroism (CD) spectra and a detailed two-dimensional NMR analysis in two solvents (trifluoroethanol and methanol) refined with molecular dynamics calculations. The X-ray diffractometric analysis of the crystals of both peptides reveals that they assume a prevalent 3_{10}-helix conformation in the solid state. This conformation is practically superimposable on that obtained from the NMR analysis of **1** in methanol. The NMR results further validate the reported CD signature of the 3_{10}-helix and the use of the CD technique for its assessment.

Keywords: helical structures · NMR spectroscopy · peptides · solvent effects · structure elucidation

Introduction

Extensive work done in several laboratories has conclusively shown that short peptides (7, 8 amino acids) rich in C^{α}-tetrasubstituted amino acids largely adopt a helical conformation.[1] This occurs not only in apolar, aprotic solvents, typically known to induce heliticity, but also in protic media and even in water.[2] The main source of this conformational preference is the geometrical constraint imposed by the two substituents at the alpha carbon atom of the C^{α}-tetrasubstituted amino acids. The helical conformation adopted by these sequences is the α or the 3_{10} conformation.[3] The two helices differ for the relative position of the C=O and NH involved in hydrogen bond formation ($i \leftarrow i+3$ and $i \leftarrow i+4$ in 3_{10}- and α-helices, respectively).[4] Consequently, the helical pitch is different (5.7 Å for the α-helix and 6.3 Å for the 3_{10}-helix) and the relative position of functional groups in the side chains varies when switching from one conformation to the other. Although the large majority of these peptides are reported to adopt the 3_{10}-helix conformation, there is mounting evidence that the solvent plays a relevant role in defining the type of helix that is formed, particularly in shorter sequences.[5] Conclusive information on the parameters that favor one or the other conformation is not yet available and, consequently, the debate remains open. Among other parameters affecting the type of conformation, save for the polarity of the solvent mentioned above, the temperature[6] and the formation of aggregates[7] should probably be taken into account. The matter is relevant because it may contribute to the understanding of the parameters affecting helical conformation in natural systems. In proteins, the α-helix largely prevails, but as the length of the

[a] Dr. M. Bellanda, Prof. Dr. S. Mammi, Dr. P. Pengo, Prof. Dr. P. Scrimin
University of Padova, Department of Chemical Sciences
35131 Padova (Italy)
Fax: (+39) 049-827-5239
E-mail: stefano.mammi@unipd.it
paolo.scrimin@unipd.it

[b] Prof. Dr. S. Geremia, N. Demitri, Prof. Dr. L. Randaccio, Prof. Dr. L. Pasquato
University of Trieste, Department of Chemical Sciences
34127 Trieste (Italy)
Fax: (+39) 040-558-3903
E-mail: randaccio@univ.trieste.it
lpasquato@units.it

[c] Dr. Q. B. Broxterman, Dr. B. Kaptein
DSM Research, Life Sciences-Advanced Synthesis & Catalysis
6160 MD Geleen (The Netherlands)

Supporting information (IR spectra of peptides **1** and **2a**, NH NMR shifts for peptide **2a**, HQMC NMR experiments for **1** and Ramachandran plots for **1a** and **2b**) for this article is available on the WWW under http://www.chemuerj.org/ or from the author.

peptide becomes shorter, the two conformations appear equally probable. An analysis of the data from an extensive study by Karle and Balaram[8] on the conformation of oligopeptides with different content of C^{α}-tetrasubstituted amino acids indicates that a six-residue helical peptide, containing only coded amino acids, is equally likely to form a 3_{10}- or an α-helix. Evidently, such a short helical peptide does not exist, but the conformational constraint provided by the C^{α} tetrasubstitution can be easily attained in the confined environment of a folded protein. In such a situation, a change of local polarity, like that induced by the modification of a substrate in the course of an enzyme-catalyzed reaction, can possibly induce a conformational change from a 3_{10}- to an α-helix. This, in turn, would alter the relative position of the functional groups in the catalytic site accounting for the dynamic binding of the substrate towards the transition state.[9] In this regard it is important to mention that there is crystal structure evidence for α- to 3_{10}-helix transition in enzymes occurring as a result of substrate binding.[10]

We have recently reported[11] preliminary data, based on circular dichroism (CD), that show how the equilibrium between the α- and 3_{10}-helix in the short peptide **1** (Ac-[Aib-L-(αMe)Val-Aib]$_2$-L-His-NH_2) correlates quite well with the empirical parameter E_T^N defining the polarity of the solvent.[12] Thus, **1** appears to adopt prevalently an α-helix conformation in water and a 3_{10}-helix conformation in isopropanol. Because of the different pitch of the two helical conformations, the length of peptide **1** varies from 15 Å in a highly polar solvent (α-helix) to 17 Å in an apolar solvent (3_{10}-helix) thus behaving like a solvent-driven molecular spring.

We are pleased to report here an NMR investigation of the conformation of this peptide and of a shorter analogue, hexapeptide **2a**, in solvents of different polarity and a comparison of the resulting conformational data with structural information obtained from single-crystal diffractometric studies. Very rewardingly, the present results fully agree with our preliminary conclusions based on the CD investigation and lend strong support to a major role played by the polarity of the solvent in controlling the type of helical conformation adopted by sterically constrained peptides.

The syntheses of heptapeptide **1** and of its precursors, hexapeptides **2a** and **2b**, have been already reported[11,13] and will not be further discussed here.

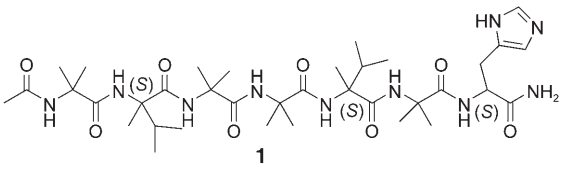

1

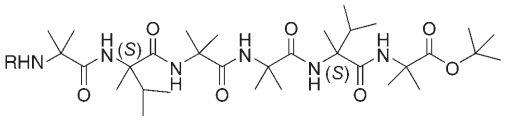

2a R = CH_3CO–
2b R = Z–

Results and Discussion

Evidence of a high helical content in peptides 1 and 2a: The helical conformation in peptides is due to the formation of intramolecular hydrogen bonds as shown in Scheme 1. Because of its structure, peptide **1** may give rise to five or six hydrogen bonds in the α- or 3_{10}-helix conformations, respectively, while the number decreases to three or four, respectively, for **2a**.

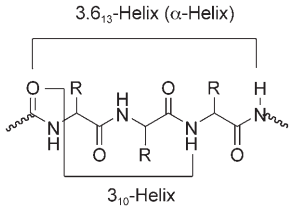

Scheme 1. Hydrogen-bond pattern in peptides according to the type of helical conformation.

Formation of secondary structures in peptide sequences is evidenced by the appearance, in their IR spectra, of new bands at lower wavelengths, both in the NH and C=O stretching regions due to the formation of intramolecular hydrogen bonds. The IR spectra in $CDCl_3$ reveal that these bands are relatively strong already in the case of hexapeptide **2a** and their intensity is not dependent on the concentration (see Supporting Information, Figure S1). This confirms that the hydrogen bonds are intramolecular and not intermolecular. Similar spectra for **1** could not be recorded due to the poor solubility of this peptide in chloroform. However, it is reasonable to believe that the hydrogen-bond content should be even higher for this longer sequence. These arguments are supported by the X-ray structural data discussed below. Further information on the presence of intramolecular hydrogen bonds in the case of peptide **2a** could be obtained with two NMR experiments. In the first one, the addition of increasing amounts of DMSO to a 2 mM solution in chloroform resulted in the significant shift of the NH proton at $\delta = 5.96$ ppm and a very limited shift of that at $\delta = 6.40$ ppm while the others remained unchanged. In the second one, the addition of CD_3OD to the very same solution of the peptide in chloroform resulted in the exchange of these two protons with the solvent, with $t_{1/2} = 10$ min and 50 min, respectively (see Figure S2 of Supporting Information). These two observations indicate that only two NH protons in peptide **2a** are not involved in hydrogen bonding. This, not only supports a highly structured conformation in chloroform for this sequence, but it suggests a 3_{10}-helix, because in this conformation only two NH are not involved in hydrogen bonding, N(1)H and N(2)H, compared to three in the case of an α-helix conformation.

In the case of peptide **1**, an accurate NMR analysis followed by simulated annealing (SA) calculations, provided the solution conformation in methanol and 2,2,2-trifluoroethanol, TFE (see below). In peptides based on C^{α}-tetrasub-

stituted α-amino acids, the lack of α-proton prevents direct scalar coupling between side chains and backbone atoms precluding the use of homonuclear scalar correlation spectra for resonance assignment. The analysis of homonuclear two-dimensional spectra is further complicated by significant signal overlap. To overcome this problem, sequential assignment of all proton and carbon resonances (see Figure S3 in the Supporting Information) was achieved by a combination of HMQC and HMBC spectra from heteronuclear CO_{i-1}–HN_i and CO_i–HN_i cross signals, as previously discussed.[14]

This information was used for the analysis of the ROESY spectra. The strong NN(i,i+1) connectivities extending along the entire sequence observed in ROESY spectra for **1** both in methanol and trifluoroethanol (Figure 1 and Supporting Information) indicate a well-defined helix.

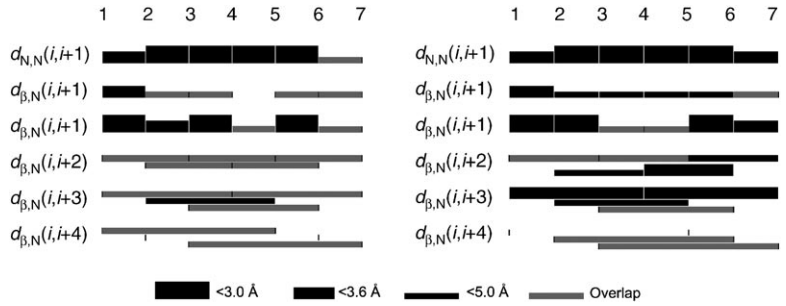

Figure 1. Summary of ROE-derived backbone distances obtained for peptide **1** in CH_3OH (left) and TFE (right). Peaks are grouped into three classes based upon their integrated volume.

The two methyl groups in the amino isobutyric acid (Aib) residues are diastereotopic, with the pro-*R* group corresponding to the H^{α} position of L-amino acids and the pro-*S* to the side chain. The analysis of the ROESY spectrum provided the correct assignment of the pro-*R* and pro-*S* geminal methyl groups (labeled β and β′, respectively, in Table 1 and Figure 2) of the four amino Aib residues present in **1**. The two diastereotopic methyls are indeed predicted to exhibit NOE interactions of different intensity with the amide protons of the same or of the preceding residue.[15] As shown in Figure 2, the two methyls of each residue can be clearly distinguished in the ^{13}C dimension of an HMQC spectrum, with the pro-*S* signal resonating at a lower field. The large ^{13}C chemical shift difference observed for the diastereotopic methyl groups is in accord with a high content of a preferred conformation for **1**.[16]

We may conclude this section by stating that peptides **1** and **2a** are highly structured in a helical conformation. This is in accord with the relevant or exclusive presence of C^{α}-tetrasubstituted amino acids in their sequence.

Dependence of the conformation of the peptides on the polarity of the solvent: The next questions we wanted to address was the type of helix formed by the peptides and the influence of the solvent on it. Our previous investigation[11] on peptide **1** was based on CD spectra and on the assumption that there was reliable information on the correct signature, not just of the α-helix but also of the 3_{10}-helix. Typically, the standard CD signal for the 3_{10}-helix is assumed to present a minimum at 208 nm and a weaker (ca. 10% of the main band) shoulder at 222 nm.[2,7,17] The shift from a 3_{10}- to an α-helix conformation is highlighted by an increase of the intensity of this negative band. In α-helices, the 222 nm band is equal in intensity or even more pronounced[18] than the one at 208 nm. The CD spectrum of peptide **1** in protic solvents of different polarity showed a strong dependence on the nature of the solvent.[11] Such a behavior is present also for the shorter peptide **2a** as shown in Figure 3. The graph reveals that, as the empirical solvent polarity parameter E_T^N increases, the molar ellipticity of the two peptides decreases. On the basis of the arguments reported above, this should be associated with a shift from a 3_{10}- to an α-helix conformation. This phenomenon is much less important for the shorter peptide **2a**.

A more accurate assessment of this very interesting behavior was needed and for this reason we analyzed the conformation of peptide **1** by NMR spectroscopy in two solvents of different polarity, that is, CH_3OH ($E_T^N=0.762$) and 2,2,2-trifluoroethanol, TFE ($E_T^N=0.898$). From the CD analysis carried out on peptide **1**, we infer that the equilibrium between the two helical conformations ($K_{\alpha/3_{10}}=[\alpha\text{-helix}]/[3_{10}\text{-helix}]$) should shift from 0.15 (CH_3OH) to 0.75 (TFE). These estimates are based on two assumptions: first, that peptide **1** is in equilibrium between only two states (i.e., the two helical conformations);[19] second, as it was mentioned before, that we know the correct CD values at 222 nm for the two helical conformations. These are reasonable assumptions but far from being proven. In any case, the data in Figure 3 indicate a relevant change of conformation of peptide **1** when it is dissolved in methanol or TFE, whatever the extent and the nature of this change is. For this reason we have chosen these two solvents for our investigation.

An unambiguous quantification of populations of each helix type by ^1H NMR methods in solution is severely limited. A ^{15}N- and carbonyl ^{13}C-labeled sample would allow the direct measurement of intramolecular hydrogen-bonding donor and acceptor atoms and their populations.[20] There are only a few NOE distances that discriminate between the two helical conformations. The most diagnostic and widely used is the distance $d_{\alpha N}(i,i+2)$, which should be 4.4 and 3.8 Å for α- and 3_{10}-helices, respectively.[21] The distance $d_{\alpha N}(i,i+4)$ is significantly shorter in the case of the α-helix, but is longer than 4 Å in both helical conformations and thus gives rise to very weak NOE intensities. However, the complete absence of this NOE might indicate a 3_{10}-helical population. Peptide **1** lacks all the α-protons with the exception of the C-terminal residue and thus these distances cannot be

Table 1. Selected geometrical parameters determined from the NMR structures in CH_3OH and TFE for **1**. Distances derived from ideal helical models are also reported as a comparison. All values were derived using the program MOLMOL.

	CH_3OH[a]	TFE[a]	3_{10}-Helix $\phi=-60°$ $\psi=-30°$	α-Helix $\phi=-57°$ $\psi=-47°$
characteristic distances				
C^β–HN ($i,i+2$) [Å]				
Aib_1C^β–Aib_3H^N	4.4	4.0	4.4	5.1
$(\alpha Me)Val_2C^\beta$–Aib_4H^N	4.9	3.9	4.2	4.9
Aib_3C^β–$(\alpha Me)Val_5H^N$	4.2	4.7	4.1	4.9
Aib_4C^β–Aib_6H^N	3.8	4.7	4.4	5.1
$(\alpha Me)Val_5C^\beta$–His_7H^N	3.7	4.3	4.3	4.9
C^β–HN ($i,i+3$) [Å]				
Aib_1C^β–Aib_4H^N	3.6	3.8	3.7	3.8
$(\alpha Me)Val_2C^\beta$–$(\alpha Me)Val_5H^N$	4.0	4.1	3.6	3.6
Aib_3C^β–Aib_6H^N	3.7	3.4	3.9	4.0
Aib_4C^β–His_7H^N	3.7	3.9	3.7	3.7
C^β–HN ($i,i+4$) [Å]				
Aib_1C^β–$(\alpha Me)Val_5H^N$	5.5	5.9	6.0	4.5
$(\alpha Me)Val_2C^\beta$–Aib_6H^N	6.2	5.2	6.1	4.6
Aib_3C^β–His_7H^N	6.2	4.4	5.9	4.5
C′–C′ ($i,i+3$) [Å]				
Aib_1CO–Aib_4CO	5.6	5.5	5.5	4.9
$(\alpha Me)Val_2CO$–$(\alpha Me)Val_5CO$	5.7	5.7	5.7	5.2
Aib_3CO–Aib_6CO	5.4	5.0	5.6	5.0
Aib_4CO–His_7CO	5.4	5.1	5.4	4.9
relative length of principal axis[b]	3.67	2.84	3.66	2.67

	backbone torsion angles [°]			
	CH_3OH		TFE	
	ϕ	ψ	ϕ	ψ
Aib_1	–	−54.0	–	−26.9
$(\alpha Me)Val_2$	−56.3	−30.1	−47.1	−34.9
Aib_3	−65.3	−47.8	−74.4	−0.2
Aib_4	−45.4	−31.1	−77.0	−51.2
$(\alpha Me)Val_5$	−59.1	−21.6	−71.3	−30.5
Aib_5	−76.9	−1.7	−66.5	−29.3
His_7	−101.9	–	−99.4	–

	helical hydrogen bonds[c]			
	CH_3OH		TFE	
	$i,i+3$	$i,i+4$	$i,i+3$	$i,i+4$
CH_3CO	3.34/142.1	3.27/170.1	2.34/162.5	4.00/129.4
Aib_1	2.59/134.7	3.21/154.2	1.73/165	3.41/147.4
$(\alpha Me)Val_2$	2.62/151.1	3.73/137.7	3.05/139	2.88/−165.6
Aib_3	1.59/171.1	3.61/137.0	3.43/127.5	2.76/148.0
Aib_4	1.89/167.9	–	2.68/149.1	–

[a] Values derived from the average structure determined upon superposition of the 20 lowest energy structures. [b] The ratio between the longest and the shortest of the molecular principal axis is indicated. [c] First value: hydrogen–acceptor distance [Å]/second value: donor–hydrogen–acceptor angle [°].

used. Nevertheless, for peptides containing C^α-tetrasubstituted amino acids, information regarding the type of helix can be extracted considering the connectivities between the NH and β-protons of the pro-*R* methyl groups, which occupy a position in space similar to that of the α-proton present in proteic L-amino acids. In particular, $d_{\beta N}(i,i+3)$ are short for

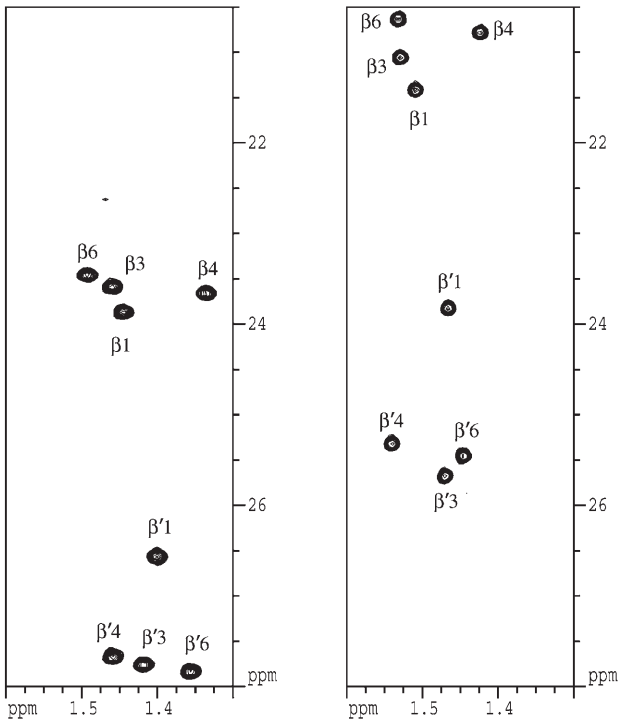

Figure 2. HMQC spectrum of peptide **1** in CH_3OH (left) and TFE (right).

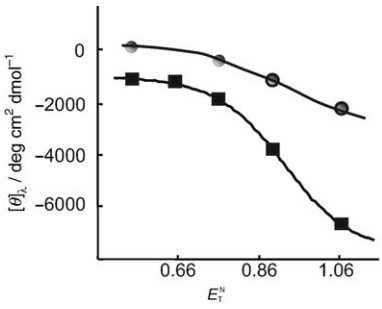

Figure 3. Molar ellipticity at 222 nm for peptides **1** (squares) and **2a** (circles) as a function of the empirical solvent polarity parameter E_T^N.

both conformations, whereas $d_{\beta N}(i,i+2)$ is significantly shorter in 3_{10}-helices and conversely, $d_{\beta N}(i,i+4)$ are short enough to give rise to observable NOEs only in the case of α-helices.[15]

The analysis of the ROESY spectrum in the two solvents provided the connectivities shown in Figure 1. Unfortunately, the poor signal dispersion results in ambiguous interpretation of the NOE connectivities. In CH_3OH, all possible $d_{\beta N}(i,i+2)$ connectivities are at least partially overlapped and their presence in the spectrum cannot be unambiguously determined even if they are potentially present along the entire sequence. Conversely, the ROE peak corresponding to $d_{\beta N}(2,6)$ is clearly not present, excluding the possibility of α-helix in the middle of the sequence at which this conformation is more favored. In TFE, $d_{\beta N}(i,i+2)$ connectivities are visible between residues 4–6 and 5–7. In this solvent, no

peak can be observed between Hβ(1) and HN(5), while the other $d_{\beta N}(i,i+4)$ connectivities remain ambiguous, so that the presence of an α-helix in the middle of peptide **1** in TFE cannot be ruled out. It is evident from this that, even if significant differences between the structures of peptide **1** in the two solvents can be observed, an unequivocal distinction between α- and 3_{10}-helical structure based on single ROE peaks does not seem possible.

The two structures could be better characterized by using the entire set of available experimentally derived distances in a molecular dynamics approach. Because of the limited quality of the NMR-derived constraints, a simulated annealing (SA) strategy, rather than distance geometry, was used to explore the conformational space. A set of structures was initially calculated in each solvent using only unambiguous NOEs; these structures were then refined introducing also the ambiguous peaks and using the r^{-6} sum function to average distances.[22] A detailed analysis of the resulting structures was performed considering different parameters, such as typical distances, torsion angles, hydrogen-bonding patterns and helix elongation (Table 1). As expected, the heptapeptide folds into a helical conformation in both solvents, but the two helices are slightly different, as can be clearly seen in Figure 4 and from the analysis of Table 1.

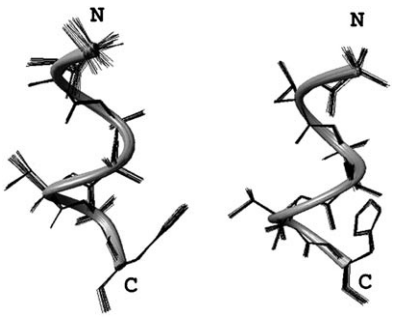

Figure 4. Backbone representation of the 20 lower energy structures obtained for peptide **1** in CH_3OH (left) and TFE (right) from SA calculations.

Although distortions from ideal geometries are evident from the dihedral angles and the calculated hydrogen-bonding network, this analysis suggests that peptide **1** adopts, prevalently, a 3_{10}-helix conformation in methanol, while in TFE it folds in a significantly less elongated structure in which both helical types are present, the α-helix being more populated in the middle of the sequence. The average backbone RMSD of the structures calculated in CH_3OH is 0.78 Å from an ideal α-helix and 0.28 Å from an ideal 3_{10}-helix. Conversely, the structures determined in TFE are closer to an ideal α-helix than to an ideal 3_{10}-helix with average RMSD of 0.58 Å and 0.76 Å, respectively. The comparison of the NMR conformers with the crystallographic structure determined for peptide **1** (see below) shows that in the solid state the heptapeptide is significantly closer to the structure determined in CH_3OH, the solvent of lower polarity, (backbone RMSD = 0.77 Å) than to the structure in TFE (backbone RMSD = 1.15 Å). This is also in good agreement with our expectation. The observed distortions in the NMR structures can probably be explained in light of the high ambiguity present in NOEs data and of the conformational averaging in solution. In fact, transitions between either helix type and random coil may take place in solution on a pico- to nanosecond timescale.[23] Thus, on the NMR timescale of milliseconds, different conformations are populated and the calculated structures represent an $\{r^{-6}\}$ average over these populations. As a consequence, a small fraction of structures with short distances between two atoms can make a large contribution to the average or, vice versa, a larger fraction of structures with longer distances can be drastically underestimated. In spite of these limitations of the NMR analysis, the calculated structures clearly confirm the presence of two different helical conformations in the two solvents (Figure 4). These results confirm those obtained from the CD analysis (see above).

One may wonder how strong is the propensity for a peptide like **1** to adopt a helical conformation as all the above data point to a highly structured sequence. Accordingly, we followed the helicity of **1** in three different solvents, methanol, TFE and hexafluoroisopropanol (HFIP) as a function of temperature. In the first solvent, as discussed above, the conformation is mostly that of a 3_{10}-helix, while in the other two the α-helix content increases. The plots in Figure 5 indicate there is no apparent change of conformation in methanol suggesting that this conformation is stable up to 330 K. The α-helix conformation seems less stable as the ellipticity in the other two solvents increases with the increase of the temperature up to the value it has in methanol suggesting that the conformation of the peptide shifts to a 3_{10}-helix. Thus, as the polarity of the solvent does, also increasing the temperature converts peptide **1** from the α- to the 3_{10}-helix (and back because the process is fully reversible) without apparent formation of disordered conformations. These experiments strongly support the conformational robustness of peptide **1** and its strong preference for a helical conformation.

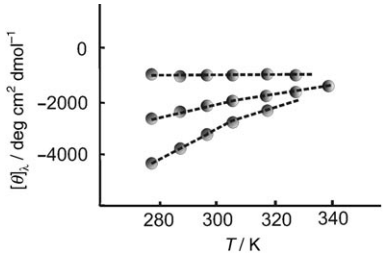

Figure 5. Temperature dependence of the molar ellipticity at 222 nm for peptide **1** in methanol, TFE, and HFIP (top, middle and bottom curve, respectively).

Solid-state structure of peptides 1 and 2b: The solid state represents, as far as solvation is concerned, an extreme condition; there is no interaction with a surrounding medium. Our anticipation was that our peptides would adopt a 3_{10}-helix conformation in the solid state, that is, the prevalent conformation in a solvent of low polarity. Crystals suitable for X-ray analysis were obtained both for peptides **1** and **2b** (see Table 2 for selected geometrical parameters obtained from the X-ray data).

Table 2. Selected geometrical parameters obtained from the X-ray structures of peptides **1** and **2b**.

	ϕ [°]	ψ [°]
compound **1**		
Aib_1	−60.80	−16.02
$(\alpha Me)Val_2$	−50.32	−26.02
Aib_3	−54.23	−15.04
Aib_4	−46.34	−30.74
$(\alpha Me)Val_5$	−45.04	−42.18
Aib_6	−54.88	−35.18
His_7	−95.08	−9.86
compound **2b**		
molecule A		
Aib_1	−57.91	−27.75
$(\alpha Me)Val_2$	−49.39	−31.05
Aib_3	−54.26	−28.73
Aib_4	−51.75	−34.45
$(\alpha Me)Val_5$	−50.98	−39.41
Aib_6	49.37	50.94
molecule B		
Aib_1	−59.91	−29.29
$(\alpha Me)Val_2$	−54.33	−25.99
Aib_3	−50.55	−32.46
Aib_4	−50.59	−36.65
$(\alpha Me)Val_5$	−57.95	−34.68
Aib_6	47.91	44.82
molecule C		
Aib_1	−55.60	−33.45
$(\alpha Me)Val_2$	−53.37	−28.83
Aib_3	−54.82	−30.11
Aib_4	−52.52	−33.37
$(\alpha Me)Val_5$	−57.46	−34.61
Aib_6	46.80	50.65
molecule D		
Aib_1	−57.36	−37.75
$(\alpha Me)Val_2$	−54.99	−29.78
Aib_3	−54.04	−30.00
Aib_4	−51.25	−35.46
$(\alpha Me)Val_5$	−51.59	−37.69
Aib_6	52.96	51.00

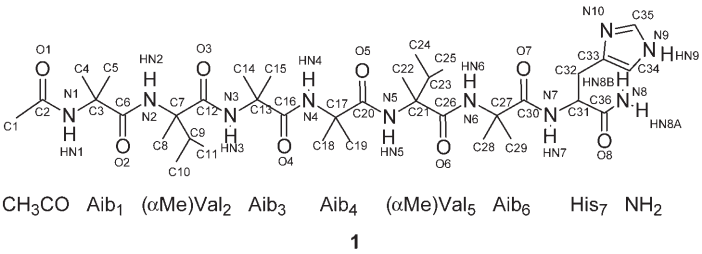

1

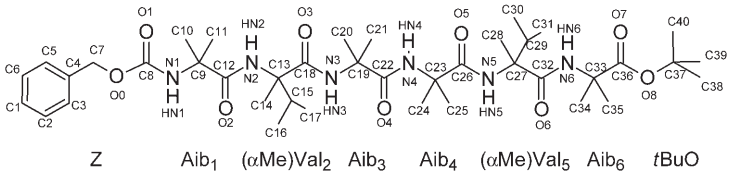

2b

Scheme 2. Numbering scheme for the atoms of **1** and **2b**.

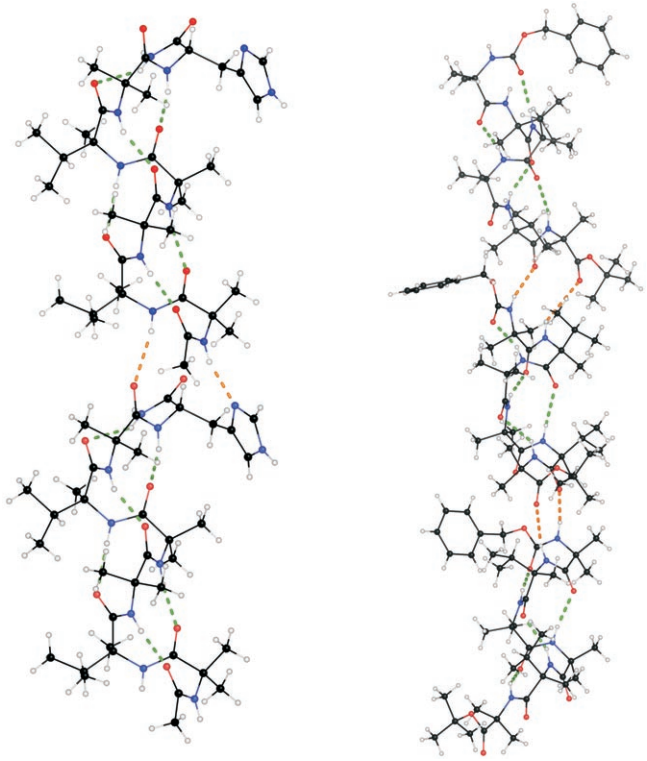

Figure 6. Left: Head-to-tail stacks of heptapeptide **1** molecules in the solid state. Right: Head-to-tail stacks of hexapeptide **2b** molecules B-C-B in the solid state. Intermolecular hydrogen bonds between the helices are indicated by orange dashed lines; intramolecular hydrogen bonds are indicated by green dashed lines.

The crystals of **1** (see Scheme 2 for the numbering scheme) consist of heptapeptide helices, stacked head-to-tail and held together by two intermolecular hydrogen bonds (see Table 3 for selected parameters) between the penultimate CO group and the N_δ imidazole atom (O7 and N10) of one helix with the first two NH groups of the following helix, which are not involved in intramolecular hydrogen bonds (Figure 6 left). The resulting stack can be considered as being made up by an alternating six residue 3_{10}-helix conformation and the seventh residue in a distorted 3_{10}-helix (Figure 6 left). The stacks are packed in the distorted hexagonal arrangement shown in Figure 7 and held together by intermolecular hydrogen bonds, between the heptapeptide terminal NH_2 group of one chain and the first carboxylic oxygen atom (O1···HN8B 2.968 Å) of the nearly parallel chain, and between the N_ε imidazole and the O6 atoms

Table 3. Experimental intra- and intermolecular hydrogen bonds in **1** in the solid state.

	D···A [Å]	∢(DHA) [°]	
intramolecular			
CH_3CO	2.932(4)	170.4	
Aib_1	2.847(4)	167.8	
$(\alpha Me)Val_2$	3.094(4)	177.3	
Aib_3	2.861(4)	155.9	
Aib_4	2.872(3)	141.9	
$(\alpha Me)Val_5$	3.160(3)	149.9	
H···A [Å]	D···A [Å]	∢(DHA) [°]	
intermolecular			
2.22	2.965(3)	141.6	N8–HN8A···O1 $(x, y-1, z+1)$
1.87	2.749(4)	175.4	N9–HN9···O6 $(x, y+1, z)$
2.08	2.924(4)	160.4	N1–HN1···N10 $(x-1, y+1, z-1)$
2.44	3.305(3)	166.3	N2–HN2···O7 $(x-1, y+1, z-1)$

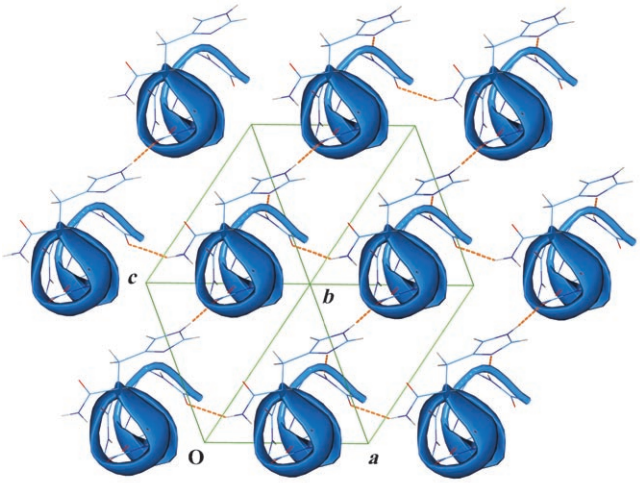

Figure 7. Crystal packing of **1** viewed along the stack axis. The hydrogen bonds among the stacks are indicated by orange dashed lines. The unit cell is shown in green.

Table 4. Intra- and intermolecular hydrogen bonds in the four crystallographically independent molecules of **2b**.

	D···A [Å]	∢(DHA) [°]		D···A [Å]	∢(DHA) [°]
intramolecular					
molecule A			molecule B		
Z	3.082(4)	167.7	Z	3.060(5)	162.1
Aib_1	2.995(4)	164.3	Aib_1	3.005(4)	167.6
$(\alpha Me)Val_2$	2.998(4)	156.7	$(\alpha Me)Val_2$	3.069(4)	158.5
Aib_3	2.932(4)	134.7	Aib_3	2.951(5)	137.1
molecule C			molecule D		
Z	2.995(4)	162.5	Z	3.015(5)	152.8
Aib_1	3.002(4)	164.7	Aib_1	2.939(5)	162.3
$(\alpha Me)Val_2$	3.086(4)	160.7	$(\alpha Me)Val_2$	3.104(4)	160.3
Aib_3	3.068(4)	140.0	Aib_3	3.022(4)	137.2

H···A [Å]	D···A [Å]	∢(DHA) [°]	
intermolecular			
molecule A			
2.08	2.860(7)	147.6	N1–HN1 A···O6 D$(x+1/2, -y+3/2, -z)$
2.76	3.344(7)	124.6	N2–HN2···O7 D$(x+1/2, -y+3/2, -z)$
2.04	2.895(7)	162.3	N1–HN1 D···O6 A$(-x+1, y+1/2, -z+1/2)$
2.33	3.098(7)	145.8	N2 D–HN2 D···O7 A$(-x+1, y+1/2, -z+1/2)$
molecule B			
1.95	2.786(7)	157.1	N1–HN1 B···O6 C$(x+1/2, -y+1/2, -z)$
2.59	3.259(7)	133.4	N2–HN2 B···O7 C$(x+1/2, -y+1/2, -z)$
1.99	2.810(7)	153.6	N1–HN1 C···O6 B$(-x+1, y+1/2, -z+1/2)$
2.85	3.600(8)	143.9	N2–HN2 C···O7 B$(-x+1, y+1/2, -z+1/2)$
molecule C			
1.99	2.810(7)	153.6	N1–HN1 C···O6 B$(-x+1, y+1/2, -z+1/2)$
2.85	3.600(8)	143.9	N2–HN2 C···O7 B$(-x+1, y+1/2, -z+1/2)$
1.95	2.786(7)	157.1	N1–HN1 B···O6 C$(x+1/2, -y+1/2, -z)$
2.59	3.259(7)	133.4	N2–HN2 B···O7 C$(x+1/2, -y+1/2, -z)$
molecule D			
2.04	2.895(7)	162.3	N1–HN1 D···O6 A$(-x+1, y+1/2, -z+1/2)$
2.33	3.098(7)	145.8	N2 D–HN2 D···O7 A$(-x+1, y+1/2, -z+1/2)$
2.08	2.860(7)	147.6	N1–HN1 A···O6 D$(x+1/2, -y+3/2, -z)$
2.76	3.344(7)	124.6	N2–HN2···O7 D$(x+1/2, -y+3/2, -z)$

(O6···HN9 2.746 Å) of another parallel chain (Figure 7). No solvent molecules were found in the crystal.

The heptapeptide secondary structure can be classified as a right-handed 3_{10} helix, if the φ and ψ angles of −95.08° and −9.86° of the N-terminal residue, corresponding to the green point in the Ramachandran plot (see Supporting Information) are excluded. The values of these angles are determined by the intermolecular hydrogen bond involving the imidazolic side chain of the N-terminal residue (see Figure 6 left). This interaction induces a relatively large spread of the other φ and ψ angles. The conformation is stabilized by six $i \leftarrow i+3$ intramolecular hydrogen bonds given in Table 3, ranging from 2.847(4) to 3.160(3) Å.

The crystals of **2b** also consist of hexapeptide helices. In this case too, the two crystallographically independent A and D helices are stacked head-to-tail along the *c* axis, but they are held together by two intermolecular hydrogen bonds (Table 4) between the last two CO groups and the first two NH groups of the following helix, which are not involved in the intramolecular hydrogen bonds (Figure 6 right). The stack consists of five residues in the 3_{10}-helix conformation with φ and ψ angles of the sixth residue falling in the region of the Ramachandran plot corresponding to a right-handed α-helix. The other two crystallographically independent B and C hexapeptides form another stack, parallel to the first ones. These stacks are packed in a distorted simple cubic arrangement as shown in Figure 8 and are held together by hydrophobic interactions among the side chains. The stack packing forms cavities where the pentane and ethyl acetate molecules, with fractional occupancies of 0.75 and 0.50, respectively, are trapped making hydrophobic interactions with the C^α side chains (Figure 8).

The four crystallographically independent hexapeptide molecules (A, B, C, D) have very similar conformations, as indicated in the Ramachandran plot (see Supporting Information). The typical folded conformation can be classified as a right handed 3_{10}-helix, if the sixth residue φ and ψ angles are excluded (about 49.3° and 49.4°, respectively). The values of the latter angles are determined by the formation of intermolecular hydrogen bonds involving this residue

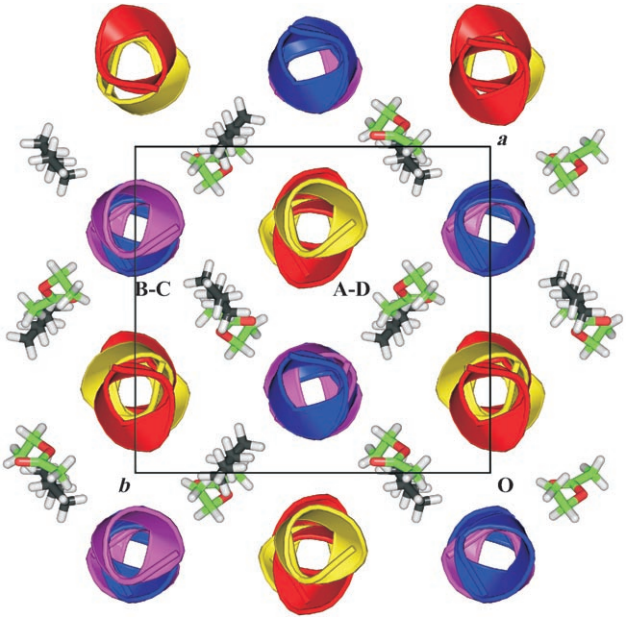

Figure 8. Crystal packing of **2b** viewed along the stack axis. The stacks are represented as ribbons and the solvent molecules as sticks.

(see above). The conformation is stabilized by four $i \leftarrow i+3$ intramolecular hydrogen bonds, reported in Table 3. The hydrogen-bond distances in the four crystallographically independent molecules are in a relatively narrow range (from 2.932(4) to 3.104(4) Å), as compared with that found in **1**. This corresponds to the clustering of φ and ψ torsion angles shown in the Ramachandran plot (see Supporting Information). Both peptides form intermolecular hydrogen bonds in the solid state that are likely replaced, in protic solvents, by hydrogen bonds with the solvent.

Conclusion

The present investigation shows conclusively that peptides **1** and **2** adopt a prevalently helical conformation both in solution and in the solid state. While in the solid state the conformation is a 3_{10}-helix, the conformation adopted in solution depends on the polarity of the solvent and switches from an α- to a 3_{10}-helix on moving from a solvent of high to one of low polarity. The NMR analysis suggests that the two peptides, in the two solutions studied, do not assume a homogeneous helical conformation and the α- and 3_{10}-helices are present within the same sequence with one of the two prevalent over the other. It was particularly rewarding to compare the two 3_{10}-helix conformations of **1** obtained from the NMR analysis in methanol and from the diffractometric study in the solid state (Figure 9): they are almost superimposable except for the two N-terminal residues, which are involved in intermolecular hydrogen bonds in the crystal. This supports a very limited conformational flexibility of this peptide even in solution. Peptides **1** and **2** constitute the first and, to date, the only example of reversible switching of peptide sequences between two helical conformations following the change of polarity of the surrounding medium.[24] Very likely, this sort of behavior is shared by other sequences of similar length and with a high content of C^{α}-tetrasubstituted amino acids.[25] It would be quite interesting to assess experimentally what is the role of the substituents in the side chains of the C^{α}-tetrasubstituted amino acids in influencing the response of the sequence to the polarity of the solvent. Our previous computational studies[11] had indicated that for a peptide of the length of **1** switching from an α- to a 3_{10}-helix, the hydrophobic interaction between the side chains is traded for an additional, intramolecular hydrogen bond. Accordingly, the modification of the hydrophobic interactions between the side chains should alter the position of the equilibrium between the two α- and 3_{10}-helix conformations. Finally, the comparison between the NMR and solid state data with the CD results indicates that this latter technique provides reliable information on the α- or 3_{10}-helix content of a sequence.

Figure 9. Overlap of the 20 lower energy structures in methanol (thin black lines) and that obtained from the X-ray analysis (thick gray line) for peptide **1**.

Experimental Section

General: The syntheses and characterizations of peptides **1** and **2a,b** have been reported elsewhere.[11,13]

Circular dichroism: The CD spectra of the peptides were recorded on a Jasco model J-715 dichrograph by using cylindrical, fused quartz cells of 1 or 0.1 mm path lengths. The data were expressed in terms of mean residue molar ellipticity. Accuracy of concentrations of peptide stock solutions were determined by quantitative amino acid analysis.

NMR experiments and structure calculation: The sample in methanol was prepared by dissolving the heptapeptide (4.19 mg; $M_W = 762.94$) in of [D_3]methanol (600 μL, $c = 9.1$ mmol L^{-1}), while for the sample in TFE, the peptide (3.14 mg) was dissolved in [D_2]TFE (550 μL, $c = 7.5$ mmol L^{-1}). The NMR experiments were performed at 298 K with a Bruker DMX 600 instrument operating at the frequency of 600 MHz for protons. Processing and evaluation of the experimental data were carried out using the programs XWinNMR 2.6 and Xeasy[26] (version 1.4).

The two-dimensional ^{1}H-^{13}C correlation spectra were carried out by using phase cycling to select coherences. The HMQC experiments[27] were recorded with 512 t_1 experiments and 16 scans with 0.7 s relaxation delay. To optimize resolution of the methyl signals, a spectral width of 6036 Hz in F1 centered at 40 ppm was used, giving a digital resolution of 11.8 Hz per point prior to zero filling. Signals from protons bound to ^{12}C were suppressed by a BIRD sequence.[28] To optimize the digital resolution, a semisoft HMBC experiment[29] was acquired with selective excitation of the carbonyl resonances by a 90° (350 μs) Gaussian-shaped pulse[30] with 1% truncation. The CO-selective HMBC experiment was performed using a long-range coupling of 7.5 Hz, a spectral width in F1 of 1811 Hz centered at 175 ppm, 200 t_1 experiments of 180 scans and a relaxation

delay of 1 s. The digital resolution in F1 prior to zero filling was 9.0 Hz per point. In both heteronuclear experiments, a spectral width of 6000 Hz centered at 4.9 ppm (methanol) or 5.4 ppm (TFE) was used in the F2 dimension.

The ROESY[31] spectrum was recorded with 700 t_1 experiments of 48 scans with 1.0 s relaxation delay. The transmitter offset was placed at 4.9 ppm (methanol) or 5.4 ppm (TFE) and a spectral width of 6000 Hz was used in both dimensions. The cross peaks analyzed were obtained with a mixing time of 150 ms and a spin lock of 8 kHz obtained by a repetitive pulse sequence.[27]

A set of interproton distances was determined for both solvent systems by a quantitative evaluation of the ROESY spectrum. Altogether, 69 (55 unambiguous and 14 ambiguous) and 95 (73 unambiguous and 22 ambiguous) NOE derived distances were determined in methanol and trifluoroethanol, respectively. The upper and lower limits of the distance restraints were generated by adding/subtracting 10% of the NOE distance, with exception of distances involving γ-protons of (αMe)Val residues where 20% of the estimated distance was added to generate the upper limits. For the calibration of the cross-peak intensities, the sequential HN(3)–HN(4) proton pair was set to a distance of 2.7 Å.

As distances were averaged by using the r^{-6} sum function[20] for equivalent protons and ambiguous NOEs, no pseudoatom correction was used.

A simulated annealing (SA) strategy was used to search the conformational space. SA calculations were performed with X-PLOR-NIH[32] 2.9.6 by using the parallhdg force field. A random conformation of the peptide backbone was generated at the beginning of each SA run in order to avoid any bias of the starting conformation on the final structures. After 100 steps of initial minimization, a total of 30 ps of high-temperature dynamics at 1500 K (random velocity initialization according to the Boltzmann distribution) was performed on this structure. The temperature was then decremented in 50 K steps to a value of 100 K during the following 30 ps of cooling. A 1000 step minimization was performed at the end of this stage. This dynamics run was followed by two stages of refinement (10 ps each) where the system was cooled from 1000 K to 100 K in 50 K decrements. An ensemble of 100 structures was generated. The 20 structures with the lowest total energy and no NOE violations above 0.5 Å were checked for further analysis. The generated structures were visualized and analyzed using the program MOLMOL[33] (version 2 K.2).

X-ray diffraction studies: Crystals of heptapeptide **1** suitable for X-ray analysis were grown in a solution of **1** in pentane and methanol, while those for hexapeptide **2** were grown from a pentane/ethyl acetate solvent mixture. Data collection was performed at the X-ray diffraction beamline of Elettra Synchrotron, Trieste (Italy) (monochromatic wavelength $\lambda =$ 0.9000 Å) using a Mar 325 image plate detector with the rotating crystal method. The crystal of **1** soaked in a drop of vaseline was mounted in a loop and flash frozen to 100 K with a nitrogen stream. The crystal of **2** was mounted on a glass fiber with glue and flash frozen to 100 K with a nitrogen stream. The diffraction data were indexed and integrated using MOSFLM[34] and scaled with SCALA.[34] The structures were solved by direct methods using SIR2002[35] and Fourier analyzed and refined by the full-matrix least-squares based on F^2 using SHELXL-97.[36] In the final refinement, all non-hydrogen atoms were treated anisotropically and the hydrogen atoms were included at calculated positions with isotropic U factors $= 1.2\ U_{eq}$. Essential crystal and refinement data are given in Table 1. CCDC 601852 (**2**) and CCDC 601853 (**1**) contain the supplementary crystallographic data for this paper. These data can be obtained free of charge from The Cambridge Crystallographic Data Centre via www.ccdc.cam.ac.uk/data_request/cif.

Acknowledgements

Financial support from the Ministry of the University and Research (Italy) is gratefully acknowledged (PRIN 2003 contract 2003037580).

[1] a) G. R. Marshall in *Intra-Science Chemistry Report, Vol. 5* (Ed.: N. Kharasch), Gordon & Breach, New York, **1971**, pp. 305–316; b) C. Toniolo, M. Crisma, F. Formaggio, G. Valle, G. Cavicchioni, G. Précigoux, A. Aubry, J. Kamphuis, *Biopolymers* **1993**, *33*, 1061–1072; c) C. Toniolo, M. Crisma, F. Formaggio, C. Peggion, *Biopolymers* **2001**, *60*, 396–419; d) E. Mossel, F. Formaggio, G. Valle, M. Crisma, C. Toniolo, M. Doi, T. Ishida, Q. B. Broxterman, J. Kamphuis, *Lett. Pept. Sci.* **1998**, *5*, 223–225.

[2] a) F. Formaggio, M. Crisma, P. Rossi, P. Scrimin, B. Kaptein, Q. B. Broxterman, J. Kamphuis, C. Toniolo, *Chem. Eur. J.* **2000**, *6*, 4498–4504; b) P. Rossi, F. Felluga, P. Tecilla, F. Formaggio, M. Crisma, C. Toniolo, P. Scrimin, *J. Am. Chem. Soc.* **1999**, *121*, 6948–6949; c) P. Rossi, F. Felluga, P. Tecilla, F. Formaggio, M. Crisma, C. Toniolo, P. Scrimin, *Biopolymers* **2000**, *55*, 496–501; d) C. Sissi, P. Rossi, F. Felluga, F. Formaggio, M. Palumbo, P. Tecilla, C. Toniolo, P. Scrimin, *J. Am. Chem. Soc.* **2001**, *123*, 3169–3170; e) A. Scarso, U. Scheffer, M. Göbel, Q. B. Broxterman, B. Kaptein, F. Formaggio, C. Toniolo, P. Scrimin, *Proc. Natl. Acad. Sci. USA* **2002**, *99*, 5144–5149.

[3] For leading studies see: a) G. R. Marshall, E. E. Hodgkin, D. A. Langs, G. D. Smith, J. Zabrocki, M. T. Leplawy, *Proc. Natl. Acad. Sci. USA* **1990**, *87*, 487–491; b) M. L. Smythe, S. E. Huston, G. R. Marshall, *J. Am. Chem. Soc.* **1993**, *115*, 11594–11595; c) M. L. Smythe, C. R. Nakaie, G. R. Marshall, *J. Am. Chem. Soc.* **1995**, *117*, 10555–10562; d) I. L. Karle, J. L. Flippenanderson, R. Gurunath, P. Balaram, *Protein Sci.* **1994**, *3*, 1547–1555; e) S. Vijayalakshmi, R. B. Rao, I. L. Karle, P. Balaram, *Biopolymers* **2000**, *53*, 84–98.

[4] C. Toniolo, M. Crisma, F. Formaggio, C. Peggion, Q. B. Broxterman, B. Kaptein, *Biopolymers* **2004**, *76*, 162–176.

[5] a) K. Otoda, Y. Kitagawa, S. Kimura, Y. Imanishi, *Biopolymers* **1993**, *33*, 1337–1345; b) M. L. Smythe, S. E. Huston, G. R. Marshall, *J. Am. Chem. Soc.* **1995**, *117*, 5445–5452; c) T. S. Yokum, T. J. Gauthier, R. P. Hammer, M. L. McLaughlin, *J. Am. Chem. Soc.* **1997**, *119*, 1167–1168; d) I. A. Topol, S. K. Burt, E. Deretey, T.-H. Tang, A. Perczel, A. Rashin, I. G. Csizmadia, *J. Am. Chem. Soc.* **2001**, *123*, 6054–6060.

[6] G. Hungerford, M. Martinez-Insua, D. J. S. Birch, B. D. Moore, *Angew. Chem.* **1996**, *108*, 356–359; *Angew. Chem. Int. Ed. Engl.* **1996**, *35*, 326–329.

[7] G. Yoder, A. Polese, R. A. G. D. Silva, F. Formaggio, M. Crisma, Q. B. Broxterman, J. Kamphuis, C. Toniolo, T. A. Keiderling, *J. Am. Chem. Soc.* **1997**, *119*, 10278–10285.

[8] I. L. Karle, P. Balaram, *Biochemistry* **1990**, *29*, 6747–6756.

[9] A. J. Kirby, *Angew. Chem.* **1996**, *108*, 770–790; *Angew. Chem. Int. Ed. Engl.* **1996**, *35*, 707–724.

[10] a) M. Gerstein, C. Chothia, *J. Mol. Biol.* **1991**, *220*, 133–149; b) C. A. McPhalen, M. G. Vincent, D. Picot, J. N. Jansonius, A. M. Lesk, C. Chothia, *J. Mol. Biol.* **1992**, *227*, 197–213.

[11] P. Pengo, L. Pasquato, S. Moro, A. Brigo, F. Fogolari, Q. B. Broxterman, B. Kaptein, P. Scrimin, *Angew. Chem.* **2003**, *115*, 3510–3514; *Angew. Chem. Int. Ed.* **2003**, *42*, 3388–3392.

[12] a) C. Reichardt, K. Dimroth, *Fortschr. Chem. Forsch.* **1968**, *11*, 1; b) C. Reichardt, *Solvents and Solvent Effects in Organic Chemistry*, VCH, Weinheim, **1988**.

[13] P. Pengo, Q. B. Broxterman, B. Kaptein, L. Pasquato, P. Scrimin, *Langmuir* **2003**, *19*, 2521–2524.

[14] S. Mammi, M. Rainaldi, M. Bellanda, E. Schievano, E. Peggion, Q. B. Broxterman, F. Formaggio, M. Crisma, C. Toniolo, *J. Am. Chem. Soc.* **2000**, *122*, 11735–11736.

[15] M. Bellanda, E. Peggion, R. Bürgi, W. Van Gunsteren, S. Mammi, *J. Pept. Res.* **2001**, 57, 97–106.

[16] R.-P. Hummel, C. Toniolo, G. Jung, *Angew. Chem.* **1987**, *99*, 1180–1182; *Angew. Chem. Int. Ed. Engl.* **1987**, *26*, 1150–1152.

[17] C. Toniolo, A. Polese, F. Formaggio, M. Crisma, J. Kamphuis, *J. Am. Chem. Soc.* **1996**, *118*, 2744–2745.

[18] a) P. Wallimann, R. J. Kennedy, D. S. Kemp, *Angew. Chem.* **1999**, *111*, 1377–1379; *Angew. Chem. Int. Ed.* **1999**, *38*, 1290–1292; b) P. Wallimann, R. J. Kennedy, J. S. Miller, W. Shalongo, D. S. Kemp, *J. Am. Chem. Soc.* **2003**, *125*, 1203–1220.

[19] This does not imply that the sequence adopts only one of the two helical conformations. Indeed the two conformations may coexist within the same peptide as also the NMR analysis suggests.
[20] a) F. Cordier, S. Grzesiek, *J. Am. Chem. Soc.* **1999**, *121*, 1601–1602; b) V. A. Jaravine, A. T. Alexandrescu, S. Grzesiek, *Protein Sci.* **2001**, *10*, 943–950; c) M. Bellanda, M. Rainaldi, Q. B. Broxterman, B. Kaptein, F. Formaggio, M. Crisma, S. Mammi, C. Toniolo, *Angew. Chem.* **2004**, *116*, 3214–3217; *Angew. Chem. Int. Ed.* **2004**, *43*, 3152–3155.
[21] K. Wüthrich *NMR of Proteins and Nucleic Acids*; Wiley: New York **1996**.
[22] M. Nilges, *Proteins Struct. Funct. Genet.* **1993**, *17*, 297–309.
[23] a) V. Y. Orekhov, D. M. Korzhnev, T. Diercks, H. Kessler, A. S. Arseniev, *J. Biomol. NMR* **1999**, *14*, 345–356; b) R. Armen, D. O. V. Alonso, V. Dagget, *Protein Sci.* **2003**, *12*, 1145–1157.
[24] Kimura et al. have recently reported on a helical peptide that exhibits two lengths in response to an applied potential and this behavior was explained with a switch from an α- to a 3_{10}-helix conformation. See: K. Kitagawa, T. Morita, S. Kimura, *Angew. Chem.* **2005**, *117*, 6488–6491; *Angew. Chem. Int. Ed.* **2005**, *44*, 6330–6333.
[25] We are indebted to Prof. C. Toniolo, University of Padova, for disclosing preliminary data from his laboratory confirming this statement.
[26] C. Bartels, T.-H. Xia, M. Billeter, P. Güntert, K. Wüthrich, *J. Biomol. NMR* **1995**, *6*, 1–10.
[27] A. Bax, R. H. Griffey, B. L. Hawkins, *J. Magn. Reson.* **1983**, *55*, 301–315.
[28] A. Bax, S. Subramanian, *J. Magn. Reson.* **1986**, *67*, 565–569.
[29] A. Bax, M. F. Summers, *J. Am. Chem. Soc.* **1986**, *108*, 2093–2094.
[30] C. Bauer, R. Freeman, T. Frenkiel, J. Keeler, A. J. Shaka, *J. Magn. Reson.* **1984**, *58*, 442–457.
[31] H. Kessler, C. Griesinger, R. Kerssebaum, K. Wagner, R. R. Ernst, *J. Am. Chem. Soc.* **1987**, *109*, 607–609.
[32] C. D. Schwieters, J. J. Kuszewski, N. Tjandra, G. M. Clore, *J. Magn. Reson.* **2003**, *160*, 65–73.
[33] R. Koradi, M. Billeter, K. Wüthrich, *J. Mol. Graphics* **1996**, 14, 51–55.
[34] "The CCP4 suite: programs for protein crystallography"Collaborative Computational Project, Number 4, *Acta Crystallogr. Sect. D* **1994**, *50*, 760–763.
[35] M. C. Burla, M. Camalli, B. Carrozzini, G. L. Cascarano, C. Giacovazzo, G. Polidori, R. Spagna, *J. Appl. Crystallogr.* **2003**, *36*, 1103.
[36] G. M. Sheldrick SHELXL-97, **1997**, University of Gõttingen (Germany).

Received: May 23, 2006
Published online: December 8, 2006

